

# A seismological reassessment of the source of the 1946 Aleutian ‘tsunami’ earthquake

Alberto M. López and Emile A. Okal

Department of Geological Sciences, Northwestern University, Evanston, IL 60201, USA. E-mail: emile@earth.northwestern.edu

Accepted 2005 December 31. Received 2005 December 18; in original form 2005 May 17

## SUMMARY

We present a re-evaluation of the seismological properties of the Aleutian ‘tsunami earthquake’ of 1946 April 1, characterized by a deceptively low conventional magnitude (7.4) in view of its catastrophic tsunami, both in the near and far fields. Relocation of 40 aftershocks show that the fault zone extends a minimum of 181 km along the Aleutian trench, in a geometry requiring a bilateral rupture from the original nucleation at the epicentre. Their spatial and temporal distribution are typical of the aftershock patterns of a large earthquake, and rule out the model of a landslide source exclusive of a dislocation. The analysis of the spectra of mantle waves favours the model of a large seismic source, with a static moment of  $8.5 \times 10^{28}$  dyn-cm, making the event one of the ten largest earthquakes ever recorded (hence the destructive tsunami in the far field), and of a slow bilateral rupture, at an average velocity of only  $1.12 \text{ km s}^{-1}$ , hence the destructive interference in all azimuths for all but the longest mantle waves. The exceptionally slow character of the earthquake is confirmed by a deficiency in radiated seismic energy expressed by the lowest value measured to date of the energy-to-moment ratio. The earthquake appears as an end member in the family of ‘tsunami earthquakes’, resulting from the combination of anomalous, but not unprecedented, parameters, such as low stress drop and rupture velocity.

**Key words:** 1946 Aleutian earthquake, slow earthquakes, tsunami earthquakes.

## INTRODUCTION AND BACKGROUND

The Aleutian earthquake of 1946 April 1 (origin time 12:29 GMT) remains a challenge to the seismological community. Despite a relatively low conventional magnitude ( $M = 7.4$  reported at Pasadena (Gutenberg & Richter 1954), it unleashed a tsunami of catastrophic proportions both in the near field, where it destroyed the Scotch Cap lighthouse and ran up to 42 m on Unimak Island (Okal *et al.* 2003a), and in the far field, where it killed 159 people in Hawaii, and inflicted damage and further casualties in the Marquesas Islands, Easter, and possibly even on the shores of Antarctica (Okal *et al.* 2002). Indeed, the 1946 event is one of the charter members of the family of so-called ‘tsunami earthquakes’, defined by Kanamori (1972) as those earthquakes whose tsunamis are disproportionately larger than expected from their seismic magnitudes, especially conventional ones such as the 20 s ‘Prague’ surface-wave magnitude,  $M_s$ , or earlier scales used by Gutenberg & Richter (1954) for historical events. Tsunami earthquakes have generally been interpreted as featuring extremely slow rupture ( $V_R$  as low as  $1 \text{ km s}^{-1}$ ), as the result of faulting either through a sedimentary wedge (Fukao 1979), or along an irregular, corrugated shallow slab interface in a sediment-starved environment (Tanioka *et al.* 1997; Polet & Kanamori 2000).

In the wake of the disastrous 1998 local tsunami in Papua New Guinea, which killed upwards of 2200 people on a 35 km stretch of coast (Synolakis *et al.* 2002), it became apparent that underwater

landslides could be unsuspected but efficient generators of locally catastrophic tsunamis. Thus, and in view of its exceptional amplitude, the source of the 1946 tsunami may have been, or may have included, an underwater landslide. This possibility, briefly mentioned by Sykes (1971) and formally presented by Kanamori (1985), had already been examined in some detail by Shepard *et al.* (1950), who disallowed it on the basis of critical features of the far-field tsunami. However, the amplitude of the near-field run-up would require a seismic slip of at least 20 m (Okal & Synolakis 2004), comparable only to that of the very largest seismic events ever recorded (Plafker & Savage 1970). Rather, a satisfactory modelling of the run-up surveyed in the near field was obtained with a  $200 \text{ km}^3$  landslide off Davidson Banks, whose existence is supported by anecdotal testimony from elderly witnesses (Okal *et al.* 2003a). While this landslide component is necessary to explain the tsunami in the near field, the question remains of the origin of the far-field tsunami and in particular of the role of the dislocative source (‘the earthquake’) in its generation. As discussed more in detail below, there remains controversy about many aspects of the seismic source, with Fryer *et al.* (2004), for example, having suggested a radical model in which there would be no detectable dislocation component, and the whole source would consist only of a giant landslide.

In this framework, the present paper offers a reassessment of the seismic properties of the 1946 event, based on main shock and

aftershock relocation, spectral analysis of mantle waves, and the estimation of radiated energy. In simple terms, we propose a model reconciling all the available seismological data with a large dislocation source featuring an anomalously slow bilateral rupture. We confirm that the landslide used by Okal *et al.* (2003a) in the near-field tsunami simulation contributes insignificantly to the observable seismic spectrum. Finally, we wish to emphasize that our purpose is not to give a model for the source of the 1946 tsunami in the far field, but rather to provide independent constraints derived from seismological data, on any future such model (Okal & Hébert 2005).

### Previous studies

The anomalous character of the earthquake can be traced to its very first description. In his administrative report of the event, the Coast Guard officer in charge of the radio station at Scotch Cap (Fig. 1) notes that the ‘second’ earthquake (i.e. the main aftershock at 12:55 GMT) was felt both stronger and shorter than the main shock

at 12:29 GMT (Sanford 1946), this combination in itself indicating a breakdown in source similitude. This testimony is upheld by an examination of the Benioff short-period records at Pasadena (Fig. 2a) showing that the *P* wave from the main shock is comparable in amplitude to that of the small 13:29 aftershock, and both smaller and lower frequency than that of the main aftershock.

The slow nature of the main shock resulted in emergent first motions, which led to difficulty both in locating the epicentre precisely, as mentioned for example by Labrousse & Gilbert (1951), and in building a focal mechanism based on first motion reports, especially given the paucity of stations available in the immediate post-war period. Hodgson & Milne (1951) proposed a mostly strike-slip solution (equivalent to  $\phi_f = 295^\circ$ ;  $\delta = 85^\circ$ ;  $\lambda = -175^\circ$ ), which Wickens & Hodgson (1967) later refined to a much greater component of normal faulting ( $\phi_f = 263^\circ$ ;  $\delta = 86^\circ$ ;  $\lambda = -60^\circ$ ). Kanamori (1972) commented on the poor resolution of the mechanism, especially given that most available stations lie near the well-constrained focal plane, and are thus nodal for *P* waves. By modelling long-period

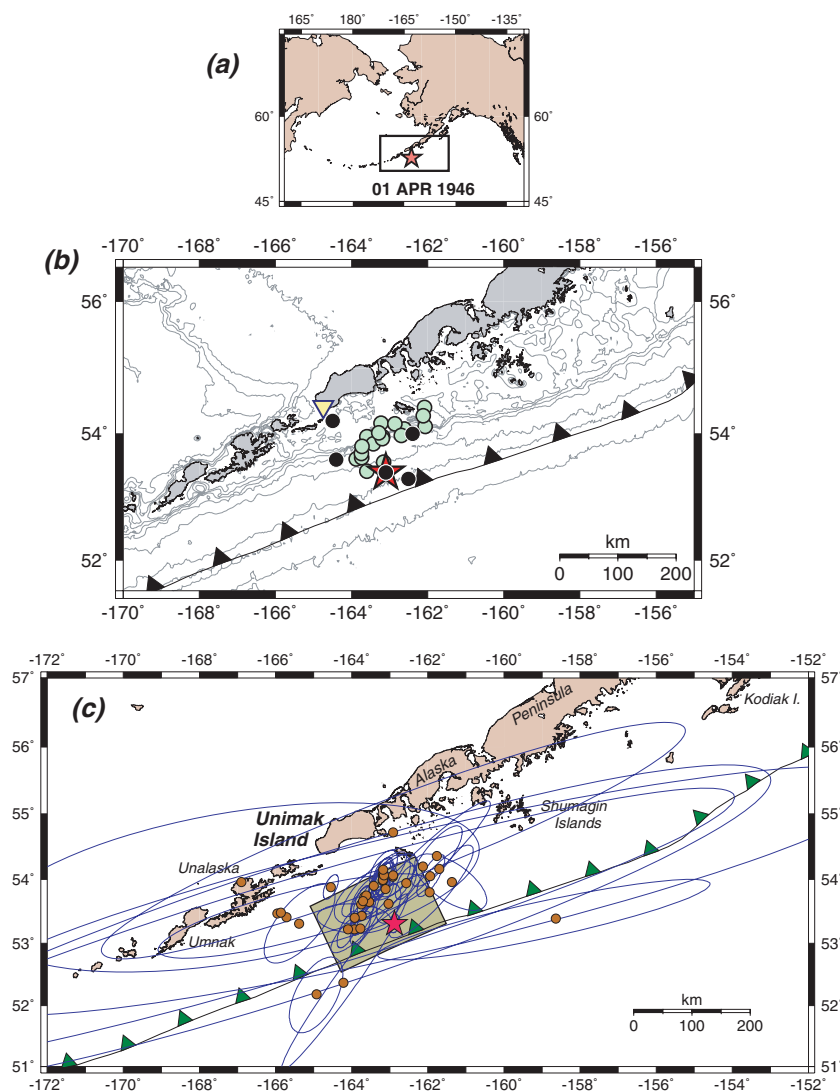


**Figure 1.** Relocation of the 1946 earthquake and its aftershocks. (a) Location map of the study area in the Northern Pacific. The box outlines the boundaries of frame (c). (b) Previous locations listed for the main shock (star) and aftershocks (solid circles) by the ISS, and for 20 aftershocks (open circles) by Sykes (1971). The inverted triangle shows the position of the eradicated lighthouse at Scotch Cap. (c) Relocations carried out in the present study for the main shock (star) and 39 aftershocks (solid circles). For each event, a Monte Carlo confidence ellipse is also plotted. The shaded rectangle is the minimum area oriented along the subduction zone and intersecting all ellipses; see text for details.

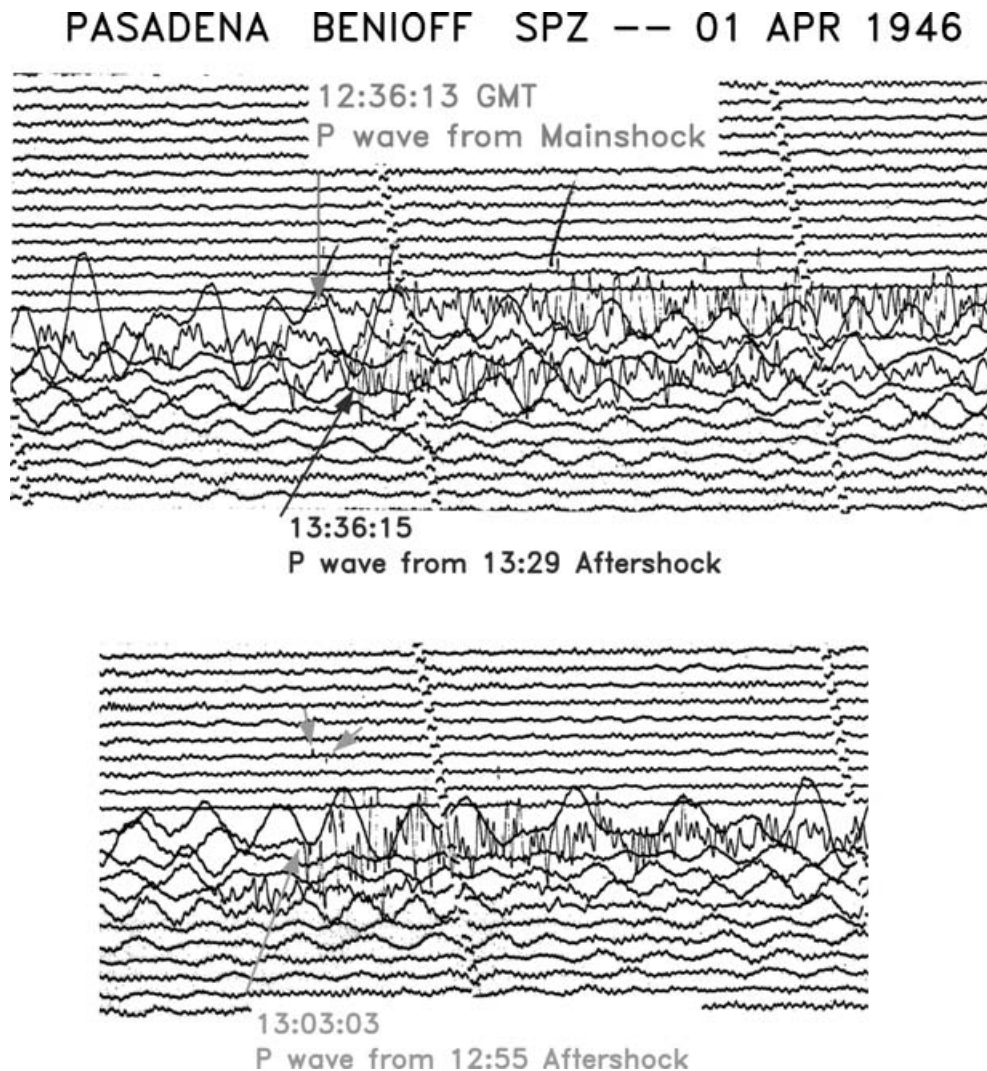


**Figure 2.** *P*-wave arrivals recorded at Pasadena on the short-period Benioff vertical seismometer. *Top*: Arrivals from the main shock (red) and 13:29 GMT aftershock (blue). Note the low-amplitude, low-frequency, and long-duration characteristics of the arrival from the main shock. *Bottom*: Arrival from the 12:55 GMT aftershock. The short green arrows point to the maximum excursion of the light spot on the paper, emphasizing the larger amplitude of the phase, as compared to that of the main shock. Note also the generally higher frequency content of the arrival. Time marks, at 1 min intervals, are affected by a clock error of 34 s, which has been corrected in the superimposed labels.

*S* waves, as well as mantle waves, Pelayo (1990) was able to overcome this difficulty, and concluded that the earthquake could be best explained as an interplate thrust event expressing the shallow-angle subduction of the Pacific plate under the Aleutian arc ( $\phi_f = 250^\circ$ ;  $\delta = 6^\circ$ ;  $\lambda = 90^\circ$ ).

Because of the slow nature of the 1946 earthquake, there also remains considerable disagreement as to the value of its seismic moment  $M_0$ , in particular in the low-frequency or static limit expected to control tsunami genesis. The exceptional disparity between the 1946 tsunami and the magnitude of its parent earthquake was noticed early on, in particular by Brune & Engen (1969), who measured the spectral density of its 100 s Love wave, which would convert to a moment of  $(1 \text{ to } 4) \times 10^{28}$  dyn-cm. Sykes (1971) relocated the main shock and 20 aftershocks of the 1946 earthquake (Fig. 1b), and described the epicentral area as 'surprisingly small [as] defined by about 15 well-located aftershocks'. A fault length of 100 km was later widely quoted as evidence for a relatively moderate seismic moment, of as little as  $8 \times 10^{27}$  dyn-cm, using Geller's (1976) scaling laws. This was probably based on the interpretation of

the 9 best located events on Sykes' (1971) fig. 5, while the rupture length suggested by his entire aftershock population would reach 160 km; furthermore, Sykes (1971) implicitly guarded against the use of scaling laws by suggesting that the earthquake featured an unusually large slip.

Kanamori (1972) proposed a moment of  $3.7 \times 10^{28}$  dyn-cm by working backwards Macdonald *et al.*'s (1947) estimate of an amplitude of 60 cm for the tsunami on the high seas through Kajiura's (1963) model of far-field weakly dispersive propagation to an estimate of  $3.75 \times 10^{16}$  cm<sup>3</sup> for the amount of water displaced at the source. We note however that this approach remains highly tentative in an era predating the development of modern technology allowing the direct detection of the tsunami wave on the high seas (González *et al.* 1991; Okal *et al.* 1999; Scharroo *et al.* 2005). Davies *et al.* (1981) proposed to apply a version of Fukao's (1979) model of rupture in an accretionary prism to reconcile the exceptional tsunami amplitude with Sykes' (1971) estimate of the fault zone. Hatori (1981) proposed a source region extending 400 km based on backtracking of traveltimes measured on Japanese tidal gauges.

Given both the potential complexity of the initial wave of a tsunami in the far field, which is widely observed as a leading depression (Tadepalli & Synolakis 1994), and the questionable frequency response of tidal gauges most often sited in harbours, this technique may not have the necessary resolution.

Pelayo (1990) relocated 11 aftershocks, obtaining a fault zone comparable to Sykes' (1971), documented an increase of moment with period, and extrapolated its static value to  $8.5 \times 10^{28}$  dyn-cm, to provide a consistent fit to his data set of *S*, Love and Rayleigh waves. Okal (1992) measured mantle magnitudes  $M_m$  ranging from 7.63 to 8.88 on a number of mantle surface waves, and suggested an increase in moment with period; he noted, however, that no multiple passages could be read on the Uppsala Wiechert records, thus advocating  $M_0 < 10^{29}$  dyn-cm, although this rule of thumb could break down for very slow earthquakes, due to the fall-off of the instrumental response. Johnson & Satake (1997) obtained a moment of  $2.3 \times 10^{28}$  dyn-cm by inversion of tidal gauge records, but noticed that their solution failed to reproduce the large run up amplitudes observed on the Hawaiian Islands; their model was constrained by Sykes' (1971) estimate of the fault length.

## RELOCATION

Our purpose in relocating the 1946 event and its aftershocks is to obtain an independent estimate of the rupture area of the event. For this purpose, we extracted from the *International Seismological Summary* (ISS) all 42 earthquakes reported in the vicinity of the main shock (in practice, less than 400 km away), for a window of one year following the event. We elect to stop our database at that point since, by then, the frequency of aftershocks has dwindled to only two in the first quarter of 1947, with none in March. We complete the data set with 11 events reported in the ISS during the same time window as 'undetermined epicentre' with a pattern of arrivals suggesting a source in the North Pacific. This initial data set makes up 53 events listed in Table 1. The importance of a careful relocation is underscored by the fact that the ISS proposes only five distinct epicentres, and defaults 35 events to the epicentral location of the main shock.

Relocations were based on *P* and occasionally *S* arrival times listed by the ISS, and were performed using the interactive iterative method of Wyssession *et al.* (1991), which features a Monte Carlo algorithm consisting of randomly injecting Gaussian noise into the data set, in order to assess the precision of the relocation; the standard deviation  $\sigma_G$  of the noise was set at 3 s, a value appropriate for 1946. Floating-depth relocations were successful in only two cases (events 30 and 52); for all other events, we used a constrained depth of 30 km. As detailed in Table 1, we eliminate 13 earthquakes from the final set of aftershocks. Nine of them were 'undetermined' epicentres unresolved by the ISS, and whose relocations range anywhere from Vancouver Island to Northern Alaska to Amchitka Island. Event 42 was assigned the main shock epicentre by the ISS, but relocates more than 600 km to the west, in the Andreanof Islands. Relocation of event 45 confirms its ISS location, 390 km to the west of the epicentral area, with a Monte Carlo ellipse not exceeding 25 km in the E–W direction.

In the case of event 41, its relocation is significantly South of the main shock, and its Monte Carlo ellipse remains seaward of the trench. Thus, we interpret it as an outboard intraplate event, doubtless triggered by the main shock as a result of stress transfer, but occurring outside the rupture area.

The resulting 39 aftershocks (Fig. 1c) represent a 95 per cent improvement in population over Sykes' (1971) data set of only 20 aftershocks. Furthermore, our relocated epicentres are distant from 3 to 126 km (mean value: 25 km) from Sykes' respective locations. These numbers clearly establish the relevance of our relocation exercise. Similarly, Pelayo (1990) had considered only 11 events. For each aftershock, the covariance of the Monte Carlo data set of relocated epicentres was then used to derive a 95 per cent confidence ellipse, which is shown in Fig. 1(c). We relocate the main shock at 53.31°N; 162.88°W (star on Fig. 1c), with an origin time of 12:29:02 GMT.

An estimate of the minimum rupture area was then computed by solving (by trial and error) for the minimum dimensions of a rectangle, oriented parallel to the trench axis (azimuth 63°), which would intersect each and every one of the aftershock ellipses. The result is a rectangular fault area measuring 181 km in length (along the trench) by 115 km in width, delimited by the shaded area in Fig. 1(c). This represents the strict minimum size of the rupture area, as determined by the full population of aftershocks. A more realistic figure based on the relocated epicentres themselves, as opposed to their Monte Carlo ellipses, would be on the order of 250 km. We will use a figure of 200 km, in round numbers, as an estimate of the length of rupture of the main shock. This estimate must be regarded as conservative.

This new result differs significantly from those of previous studies which limited the fault length to 100 km, based on a minimalistic interpretation of Sykes' (1971) aftershock data plotted in his Fig. 5. This has some important consequences, which we discuss in some detail. First, the length of rupture required by this new model is double that proposed by previous authors (Sykes 1971; Pelayo 1990). The minimum width of the horizontal projection of the fault zone, 115 km, is, on the other hand, essentially unchanged from these authors' conclusions.

Second, a comparison between Sykes' (1971; Fig. 5) and our Fig. 1(c) shows that the increase in fault length comes almost entirely from aftershocks located to the WSW of the main shock. As such, our aftershock population does not require extending the 1946 rupture area East of 162°W (at 53.8°N), and thus could leave the so-called Shumagin gap (Jacob 1984) unaffected. By contrast, it reduces by at least 75 km (leaving it only 125 km wide) the Unalaska gap, which separates the rupture zones of the 1957 and 1946 earthquakes.

This new estimate of the aftershock area, clearly featuring a substantial extent laterally along the subduction zone, is also incompatible with the recent model by Fryer *et al.* (2004), in which the main seismic event at 12:29 GMT on 1946 April 1 would be a major landslide, perhaps triggered by a small earthquake, whose size would remain too small to contribute substantially to the available seismic records. A significant problem with such a model is the family of 39 aftershocks listed in Table 1: they would have to be landslide replicas, or 'afterslides', a phenomenon of which we know very little in terms of existence and statistics, but certainly unlikely to occur as much as 150 km away from the main event, especially under the continental shelf, in a zone essentially lacking any slope.

Rather, it is clear that the 40 events listed in Table 1 have the 2-D geographical repartition expected of the main shock and aftershocks of a major earthquake; furthermore, Fig. 3 shows that their temporal distribution is also well fitted by a modified Omori law with an exponent  $p = 1.12$ , well within the range of that parameter for typical earthquake sequences (Utsu *et al.* 1995). We conclude that the Aleutian event at 12:29 GMT on 1946 April 1 was indeed a genuine, if slow, dislocative source, in other words an earthquake.

Table 1. Relocation parameters of the 1946 Aleutian event and its aftershocks.

Event Number	Date	Original (ISS) location			Relocation			Error ellipse					
		Time	Latitude (°N)	Longitude (°E)	Latitude (°N)	Longitude (°E)	Depth (km) ( <i>d</i> )	Origin time GMT	Number of stations	$\sigma$ (s)	Semi-major axis (km)	Semi-minor axis (km)	Major axis azimuth (°)
1	1946 Apr 1	12:28	53.40	-163.10	53.31	-162.88		12:29:01.6	92	2.09	16	9	8
<i>Main shock</i>													
2	1946 Apr 1	12:52	53.40	-163.10	54.20	-162.13		12:52:49.8	20	0.95	160	25	46
3	1946 Apr 1	12:55	53.40	-163.10	54.07	-163.18		12:55:52.4	45	0.96	29	14	22
4	1946 Apr 1	13:28	53.40	-163.10	53.80	-161.95		13:28:59.7	34	4.34	105	26	42
5	1946 Apr 1	13:34	53.40	-163.10	53.41	-165.71		13:34:23.3	16	0.95	243	43	76
6	1946 Apr 1	13:40	53.40	-163.10	54.72	-162.91		13:40:38.1	15	1.48	529	69	69
7	1946 Apr 1	14:47	53.40	-163.10	52.37	-164.22		14:47:44.0	12	0.60	192	20	35
8	1946 Apr 1	15:50	53.40	-163.10	53.22	-163.93		15:50:36.6	27	1.90	55	18	45
9	1946 Apr 1	16:59	53.40	-163.10	53.43	-163.74		16:59:18.0	48	2.23	36	14	25
10	1946 Apr 1	18:57	53.40	-163.10	53.65	-163.54		18:57:40.0	78	2.59	19	10	13
11	1946 Apr 2	00:58	53.40	-163.10	53.73	-163.67		0:58:29.0	13	1.63	61	32	51
12	1946 Apr 2	04:13	53.40	-163.10	53.61	-163.75		4:13:43.8	52	2.59	34	13	25
13	1946 Apr 2	05:38	53.40	-163.10	53.94	-162.57		5:38:21.2	47	2.43	32	13	26
14	1946 Apr 2	05:57	53.40	-163.10	54.05	-161.94		5:57:17.8	48	2.72	41	14	30
15	1946 Apr 2	13:04	53.40	-163.10	53.75	-163.62		13:4:24.8	33	2.07	40	16	35
16	1946 Apr 2	14:27	53.40	-163.10	54.04	-162.92		14:27:33.7	19	1.80	52	24	47
17	1946 Apr 2	16:30	53.40	-163.10	53.66	-163.70		16:30:29.6	53	1.95	30	12	22
18	1946 Apr 3	08:58	53.40	-163.10	53.98	-163.19		8:58:39.7	44	2.35	33	12	18
19	1946 Apr 4	07:15	53.40	-163.10	53.96	-161.37		7:15:26.8	6	0.82	72	32	-54
20	1946 Apr 4	16:31	53.40	-163.10	53.62	-163.03		16:31:13.3	23	2.59	36	18	22
21	1946 Apr 4	21:25	53.40	-163.10	53.99	-163.18		21:25:46.8	36	1.52	34	17	33
22	1946 Apr 5	06:55	53.40	-163.10	53.40	-163.92		6:55:46.0	9	1.22	64	26	-86
23	1946 Apr 6	04:52	53.40	-163.10	53.23	-163.77		4:52:38.8	51	2.85	32	13	26
24	1946 Apr 7	22:52	53.40	-163.10	53.31	-165.38		22:52:49.3	14	2.01	85	37	40
25	1946 Apr 8	15:17	53.40	-163.10	53.90	-163.42		15:17:11.8	16	1.07	76	22	45
26	1946 Apr 8	17:36	53.40	-163.10	54.06	-163.15		17:36:35.0	24	1.72	34	14	17
27	1946 Apr 9	07:08	53.40	-163.10	53.39	-158.64		7:8:44.9	13	0.53	296	32	78
28	1946 Apr 13	05:19	53.40	-163.10	53.47	-165.95		5:19:04.9	10	1.17	859	115	72
29	1946 Apr 13	08:07	53.40	-163.10	53.48	-165.86		8:7:28.2	10	0.94	809	84	73
30	1946 Apr 14	04:24	53.40	-163.10	53.96	-166.90	29	4:24:32.5	11	0.70	428	129	80
31	1946 Apr 19	12:04	53.40	-163.10	54.16	-161.70		12:4:31.9	10	0.98	844	103	77
32	1946 May 2	05:40	53.40	-163.10	54.36	-161.76		5:40:57.3	14	1.47	64	21	38
33	1946 Jun 9	06:56	53.40	-162.40	54.06	-162.91		6:56:12.0	18	0.95	41	24	33
34	1946 Aug 2	01:37	53.40	-163.10	54.15	-163.17		1:38:03.0	23	2.21	36	17	31
35	1946 Sep 16	07:47	54.20	-164.50	52.18	-164.92		9:56:24.2	14	3.72	75	36	28
36	1946 Oct 30	05:56	53.60	-164.40	53.88	-164.55		7:47:36.8	100	2.32	23	10	25
37	1946 Nov 12				53.22	-164.10		5:56:24.0	50	2.27	35	13	25
38	1946 Dec 25				53.85	-163.11		6:14:14.9	18	1.26	63	26	46
39	1947 Jan 23	15:57	53.30	-162.50	53.26	-162.32		15:57:47.0	44	2.39	56	19	32
40	1947 Feb 15	01:07	53.40	-163.10	53.44	-163.27		1:7:55.4	23	2.00	55	33	65

Table 1. (Continued.)

Event Number	Date	Original (ISS) location		Relocation			Error ellipse							
		Time	Latitude (°N)	Longitude (°E)	Latitude (°N)	Longitude (°E)	Depth (km) ( <i>a</i> )	Origin time GMT	Number of stations	$\sigma$ (s)	Semi-major axis (km)	Semi-minor axis (km)	Major axis azimuth (°)	
41	1946 Apr 1	15:20	53.40	-163.10	52.00	-165.21	Other events	15:20:19.0	23	1.55				
42	1946 Apr 15	07:06	53.40	-163.10	52.95	-172.75		07:05:30.6	12	1.00				
43	1946 Apr 17				70.05	-140.57		14:07:21.0	11	2.82				
44	1946 Jun 11				50.07	-126.96		08:00:06.9	13	3.93				
45	1946 Jul 12		53.80	-168.90	53.83	-168.74		12:21:53.5	48	2.29				
46	1946 Jul 26				49.29	176.47		04:12:33.8	13	1.94				
47	1946 Jul 28				69.61	-138.74		08:00:58.0	15	2.41				
48	1946 Jul 28				50.30	179.44		22:20:12.1	13	2.18				
49	1946 Jul 30		53.40	-163.10	54.71	-164.27		18:36:16.2	14	2.17				
50	1946 Sep 11				69.22	-141.51		02:04:32.5	9	1.74				
51	1946 Oct 15				53.11	-133.87		14:55:17.0	13	1.56				
52	1947 Mar 17				63.78	-147.38		05:29:15.1	14	1.55				
53	1947 Mar 24				53.88	-172.27		15:40:56.9	14	1.00				

<sup>a</sup>Depth is listed only when successfully inverted. Otherwise, it was constrained at 30 km during the relocation.

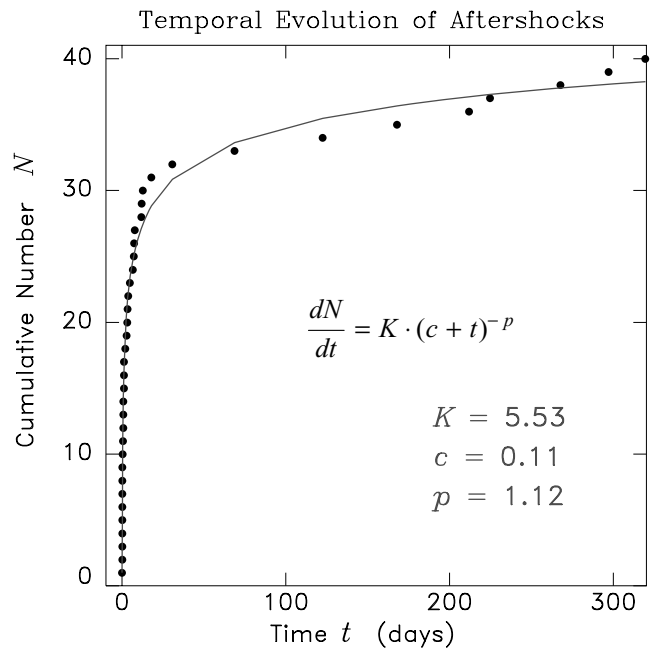


Figure 3. Temporal distribution of the main shock and 39 aftershocks of the 1946 Aleutian earthquake listed in Table 1. The individual dots show the cumulative number  $N$  of aftershocks recorded after a time  $t$  (abscissa; in days after the main shock). The solid line fits a modified Omori formula of the form  $K \cdot (c + t)^{-p}$  to the rate of occurrence of aftershocks, equivalent to the derivative  $dN/dt$ .

A further consequence of the enlarged geometry of rupture is the location of the main shock epicentre, interpreted as the locus of initiation of faulting, away from the edges of the fault zone. As such, it requires a bilateral rupture propagating in both directions away from the epicentre, a geometry already advocated, albeit on a smaller scale, by Pelayo (1990). In turn, and as detailed below, this results in directivity patterns featuring destructive interference at all azimuths. Thus, we anticipate that its static moment would have been systematically underestimated, in all azimuths and for all but waves of the very lowest frequencies (expected to be poorly recorded by historical instruments).

## WAVEFORM ANALYSIS

### Records used

Table 2 lists the eleven records used for waveform analysis in the present study. A particularly important one was obtained on the Pasadena Benioff 1-90 seismograph system. With its two very different periods, this instrument featured an improved response at long periods (Benioff 1935), and can be considered a precursor to the broad-band systems developed in the past decades. The 1946 earthquake was well recorded on all three components of the system at PAS (Fig. 4). We complemented the Pasadena seismograms with a few records featuring high-quality recording on instruments selected for their response characteristics (e.g. the Benioff 1-60 seismograph at Weston, a close sibling of the PAS one) and for excellent documentation at the archiving station, providing undisputed information of their magnification and frequency response.

The PAS vertical record was hand digitized following optical magnification by a factor of 8, and equalized to a sampling of 0.1 s, over a long window lasting over 3.5 hr. This allows the detailed study of several aftershocks as well as of the main shock. The north-south

**Table 2.** List of records used in the present study.

Station		Distance (°)	Azimuth (°)	Backazimuth (°)	Instrument	Phase
Code	Name					
PAS	Pasadena, California	36.77	103	315	Benioff 1-90	$G_1$
PAS	Pasadena, California	36.77	103	315	Benioff 1-90	$R_1$
PAS	Pasadena, California	323.23	293	135	Benioff 1-90	$R_2$
PAS	Pasadena, California	396.77	103	315	Benioff 1-90	$R_3$
WES	Weston, Massachusetts	58.21	60	315	Benioff 1-60	$G_1$
WES	Weston, Massachusetts	301.79	240	135	Benioff 1-60	$G_2$
WES	Weston, Massachusetts	418.21	60	315	Benioff 1-60	$G_3$
UPP	Uppsala, Sweden	67.01	360	0	Wiechert	$R_1$
UPP	Uppsala, Sweden	67.01	360	0	Wiechert	$G_1$
DBN	De Bilt, The Netherlands	74.30	8	353	Golitsyn	$R_1$
CHR	Christchurch, New Zealand	98.92	198	15	Golitsyn	$G_1$

component shows a prominent first passage of the Love wave,  $G_1$ , which was isolated and digitized at a sampling of 1 s. Records at other stations were also hand digitized at a 1 s sampling.

### Mantle magnitude $M_m$ and Seismic Moment $M_0$ : Initial measurements

All eleven records listed in Table 2 were initially processed using Okal & Talandier's (1989) mantle magnitude algorithm,  $M_m$ . We recall that the mantle magnitude  $M_m$  is designed to match the quantity  $\log_{10} M_0 - 20$ , where  $M_0$  is in dyn-cm, and is computed at each frequency from the spectral amplitude  $X(\omega)$  of either Rayleigh or Love mantle waves through

$$M_m = \log_{10} X(\omega) + C_D + C_S + C_0, \quad (1)$$

where  $C_D$  is a distance correction,  $C_S$  a source correction, and the constant  $C_0 = -0.90$  (if  $X$  is in  $\mu\text{m}\cdot\text{s}$ ) is justified theoretically (Okal & Talandier 1989). This approach has the advantage of being insensitive to parameters such as centroid depth and focal mechanism. As documented in Fig. 5, measurements of  $M_m$  at most stations in the data set feature a very strong dependence on frequency, with average values as large as  $M_m = 8.5$  for  $T = 273$  s, but only 7.2 at  $T = 51$  s. This trend confirms the slow character of the source of the 1946 earthquake, and in particular the gross underestimation of its true size by traditional magnitude measurements, such as the value of 7.4 reported by Gutenberg & Richter (1954).

### Modelling the source time function and constraining the static moment

We further constrain the source properties of the 1946 Aleutian earthquake by modelling the evolution with frequency of the spectral amplitude  $X(\omega)$  at selected stations. We recall that the latter will be controlled by the combination of

- (i) the static moment  $M_0$  of the earthquake;
- (ii) the centroid depth  $h$  and geometry  $(\phi_f, \delta, \lambda)$  of the focal mechanism;
- (iii) the rise time  $\tau_c$  of the source characterizing the time taken by the rupture at an individual point along the fault and
- (iv) the geometry and kinematics of the propagation of the rupture along the fault plane, the latter representing the so-called 'directivity function' introduced by Ben-Menahem (1961).

Our approach is to use our relocation results to constrain (iv) to a small number of possible geometries, and to further explore combinations of focal depths and mechanisms (ii). For each record under study, we define a best-fitting static moment  $M_0$  (i) and rise

time  $\tau_c$  (iii) by using Silver & Jordan's (1983) algorithm to fit a curve of the form

$$M_m(\omega) = M_m(0) - \log_{10} \left[ 1 + \frac{\omega^2 \tau_c^2}{8} \right] \quad (2)$$

(adapted from their eq. 22), to the curves shown in Fig. 5 which describe the fluctuation of  $M_m$  with frequency, while keeping track of the quality of the resulting fit for each set of parameters (ii).

An example of this procedure, in the case of the first Rayleigh passage ( $R_1$ ) at Pasadena, is illustrated in Fig. 6 and detailed below. The  $M_m$  algorithm consists of correcting the raw spectral amplitude  $X(\omega)$  for distance and excitation. The distance correction  $C_D$  involves the effects of both geometrical spreading and anelastic attenuation. As detailed by Okal & Talandier (1989), the excitation correction  $C_S$  is averaged over focal mechanism and centroid depth and merely corrects for the general evolution with frequency of mantle Rayleigh wave excitation by a double couple. The resulting values of  $M_m(\omega)$  are the ones shown in Fig. 5, and are plotted as solid dots along the short-dashed line in Fig. 6. Note the strong dependence with frequency.

The next step in our procedure is to carry out a directivity correction. We base our fault rupture model on the mapping of the fault zone resulting from our aftershock relocation. We consider a bi-lateral rupture extending  $L_1 = 80$  km ENE and  $L_2 = 120$  km WSW from the relocated epicentre of the main shock, with the fault rupture trending  $\phi_R = N63^\circ\text{E}$ , which expresses the general tectonic framework of the local subduction, according to the geometry of Fig. 1(c). We use a rupture velocity  $V_R = 1.12$  km  $\text{s}^{-1}$ , as constrained below, and in general agreement with those determined from detailed source tomography of other, modern, tsunami earthquakes for which large digital waveform databases are available (e.g. Kikuchi & Kanamori 1995). At a station in azimuth  $\phi_s$ , and for a mantle wave with phase velocity  $c(\omega)$ , the directivity function, adapted from Ben-Menahem (1961) to the case of a bilateral rupture is simply:

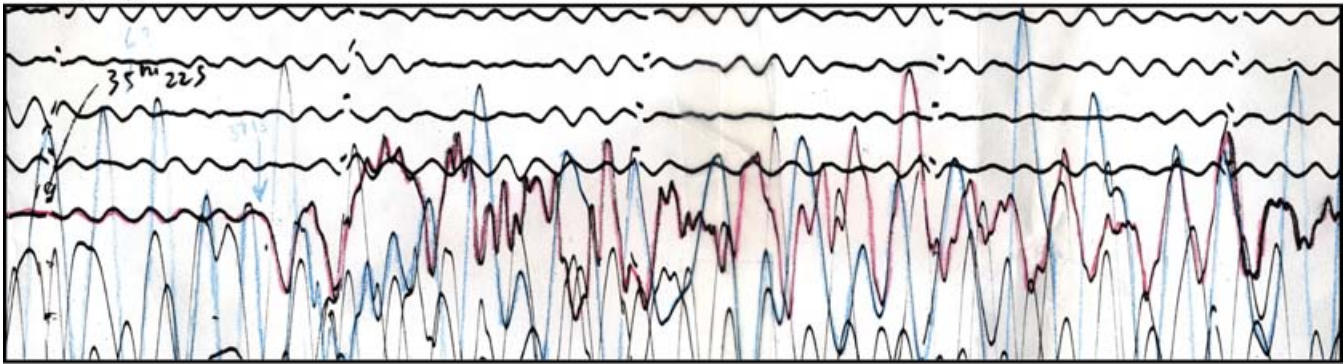
$$\begin{aligned} DIR(\phi_s; \omega) &= \left| \frac{L_1}{L_1 + L_2} \cdot \text{sinc} \left[ \frac{\omega L_1}{2c} \left( \frac{c}{V_R} - \cos \phi \right) \right] \cdot e^{-\frac{i\omega L_1}{2c} \left( \frac{c}{V_R} - \cos \phi \right)} \right. \\ &\quad \left. + \frac{L_2}{L_1 + L_2} \cdot \text{sinc} \left[ \frac{\omega L_2}{2c} \left( \frac{c}{V_R} + \cos \phi \right) \right] \cdot e^{-\frac{i\omega L_2}{2c} \left( \frac{c}{V_R} + \cos \phi \right)} \right| \end{aligned} \quad (3)$$

where sinc represents the circular sine function:  $\text{sinc } X = \sin X/X$ , and  $\phi = \phi_s - \phi_R$ . At each frequency, the correction

$$C_{DIR} = -\log_{10} DIR, \quad (4)$$

## PASADENA 01 APRIL 1946

(a)



(b)

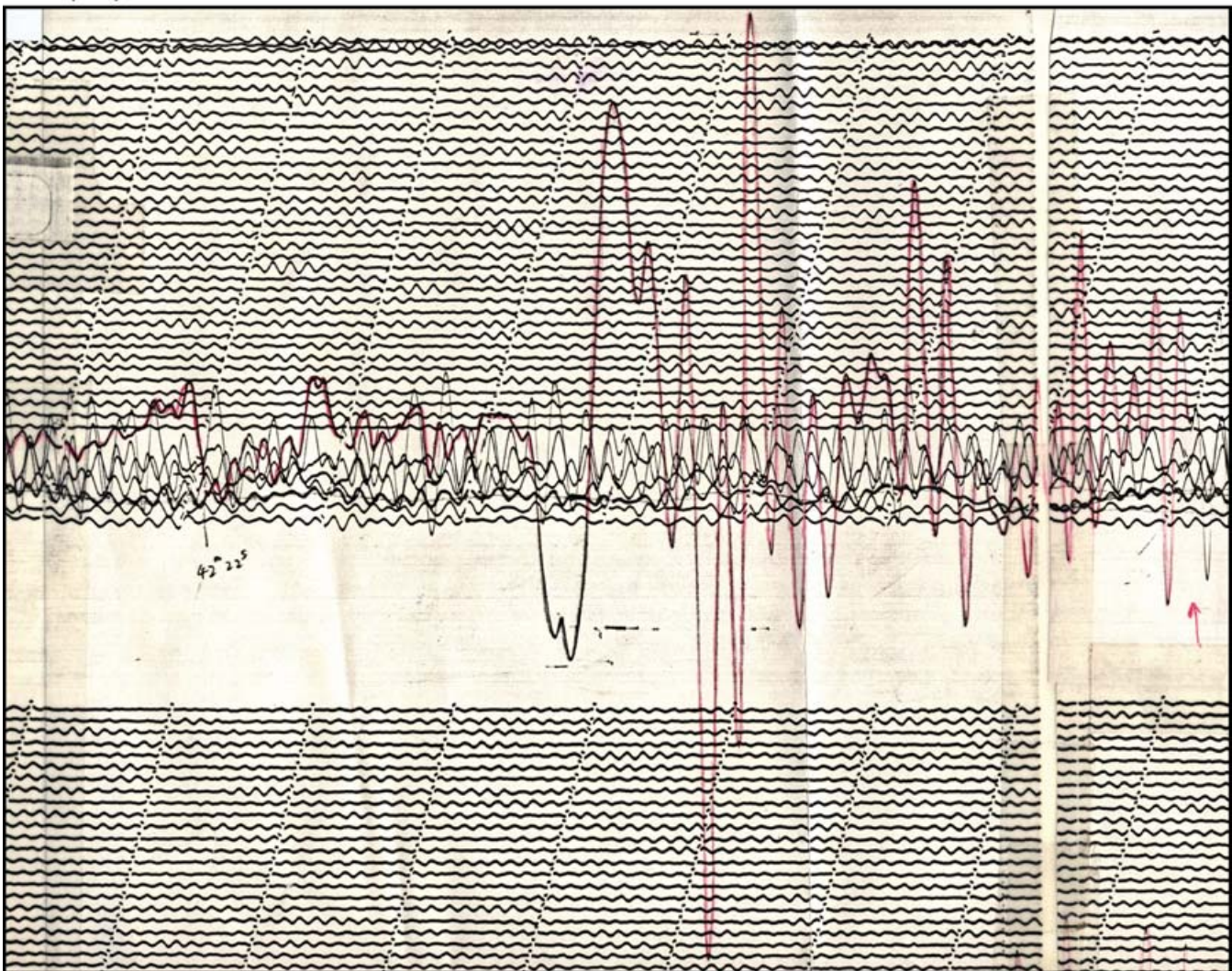


**Figure 4.** Recordings of the 1946 Aleutian earthquake on the 1-90 Benioff seismographs at Pasadena. Time marks are uncorrected minutes. (a)  $P$ -wave recording on the vertical instrument. The window shown is approximately 270 s in duration. The relevant trace is outlined in red pencil. Note the remarkable deficiency of the record in high-frequency energy. (b) Love wave  $G_1$  recorded on the north-south component. The window shown is approximately 500 s in duration.

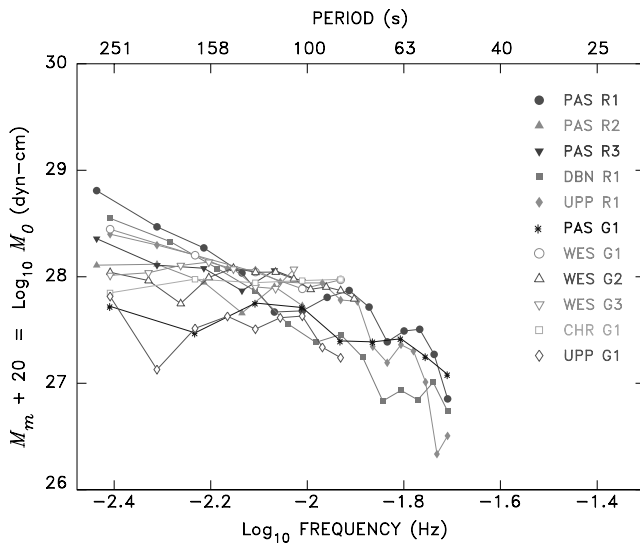


**Figure 5.** Estimates of the mantle magnitude  $M_m$  for the 11 records used in this study. For each record, the symbols represent the raw calculation of the mantle magnitude  $M_m$  according to eq. (1). For a standard source with corner frequencies greater than the sampling frequencies, the value of  $M_m$  at each station should be constant (i.e. the individual lines horizontal). The observed strong negative trend with frequency is indicative of source slowness.

is applied to the individual value of  $M_m$  and the resulting values are plotted as the squares along the intermediate-dashed line in Fig. 6. Note the significant decrease in the (negative) slope of  $M_m$  with frequency.

Finally, a focal mechanism (and depth) correction is applied by considering the detailed effect of those parameters, rather than taking their average value  $C_S$ , with the results shown in Fig. 6 as the short-dashed lines connecting the individual triangles, for a centroid depth of 20 km, and the mechanism  $\phi_f = 243^\circ$ ;  $\delta = 10^\circ$ ;  $\lambda = 90^\circ$ , adapted from Pelayo (1990). This procedure is equivalent to the transition from  $M_m$  to the so-called ‘corrected’ magnitude  $M_c$ , as described in detail by Okal & Talandier (1989), to which the reader is referred. Note the further reduction in the dependence of mantle magnitude with frequency. At this stage, the results are expected to reflect only the rise time  $\tau_c$  of the earthquake source, and the individual values of the corrected spectral amplitudes are fit using a least-squares procedure with a function of the type (2) (Silver & Jordan 1983). The best-fitting curve, corresponding in this case to  $M_0 = 1.22 \times 10^{29}$  dyn-cm and  $\tau_c = 54$  s, is shown as the solid line in Fig. 6. The quality of this fit can be computed as the root-means-square of the logarithmic misfits between the solid curve and the individual triangles in Fig. 6.

The procedure is then extended to the other records under study (e.g.  $R_3$  at PAS in Fig. 6b) and also iterated for a number of different models of focal and rupture geometry. In particular, the value  $V_R = 1.12 \text{ km s}^{-1}$  is constrained by fitting the prominent spectral hole in the phase  $R_2$  at Pasadena (Fig. 7), which is found to be crucially sensitive to the exact value of  $V_R$ . Individual sets of  $(M_0; \tau_c)_i$  values, obtained for each of the eleven records (indexed  $i = 1$  to 11), are themselves best fit in the range 3.6–10 mHz by a single function of the type (2), yielding the final static moment  $M_0 = 8.5 \times 10^{28}$  dyn-cm and rise time  $\tau_c = 40$  s. The precision of this solution can be estimated from the standard deviation,  $\sigma_M = 0.3$  logarithmic units, of the quantities  $\log_{10}(M_0)_i$  for the various records. Furthermore, we found that small variations in focal mechanism orientation ( $\approx 10^\circ$ ) or centroid depth (down to 20 km)

affect the final static moment only marginally, as  $\log_{10} M_0$  remains within  $\sigma_M$ . We thus regard the above value of the static moment as robust.

This value,  $M_0 = 8.5 \times 10^{28}$  dyn-cm, is remarkably identical to that preferred by Pelayo (1990), and the combination of  $M_0$  and  $\tau_c$  predicts an apparent  $M_0$  of  $7.1 \times 10^{28}$  dyn-cm at 256 s, in good agreement with the additional measurement at Florissant, quoted by Okal (1992) but not used in the present study. At 100 s, the apparent moment would be  $4.4 \times 10^{28}$  dyn-cm, which is only 10 per cent larger than the maximum values inferred from Brune & Engen’s (1969) measurements of Love wave spectral densities. The static value of  $M_0$  also confirms that the 1946 Aleutian earthquake is among the 10 largest seismic events ever recorded, and justifies qualitatively that its far-field tsunami should have been catastrophic.

Because the near-field tsunami requires generation by a landslide, it is imperative to address the question of the latter’s seismic signature. In Okal (2003), we showed that both the Rayleigh and tsunami spectra excited in the far field by a landslide representative of the 1946 near-field tsunami source were 1.5 and 1 orders of magnitude smaller than their respective counterparts for an appropriate dislocation source. Fig. 8 is adapted from Fig. 1 of Okal (2003), with the seismic moment updated to its definitive value of 8.5 (as opposed to 5)  $\times 10^{28}$  dyn-cm, and the landslide volume to the 200 km<sup>3</sup> used by Okal *et al.* (2003a). It shows that the Rayleigh wave spectra from a slow earthquake and a landslide (respectively of order  $\omega^{1/2}$  and  $\omega^{3/2}$ ) differ irrevocably at the lowest mantle frequencies. We conclude that the landslide remains essentially invisible in the seismic record; the figure also predicts schematically its minor contribution to the far-field tsunami.

### Estimated radiated energy $E^E$ and parameter $\Theta$

The vertical Benioff 1-90 record of the generalized  $P$  wave at Pasadena was processed through Newman & Okal’s (1998) algorithm to obtain the estimated energy  $E^E$ . We recall that this quantity is derived from the concept of radiated energy introduced by Boatwright & Choy (1986), but does not involve corrections for exact hypocentral depth and focal mechanism, thus providing a robust estimate of the high-frequency characteristics of the source while preserving the philosophy of a magnitude measurement. Newman & Okal (1998) further introduced a dimensionless parameter  $\Theta = \log_{10}(E^E/M_0)$ , characteristic of the slowness of a seismic source. While most scaling laws predict  $\Theta = -4.90$ , slow events such as ‘tsunami earthquakes’ feature  $\Theta \leq -6$ . Although originally developed for modern, digitally recorded data, Okal & Kirby (2002) later showed that the algorithm can be extended to historical records obtained on relatively broad-band instruments, such as the Pasadena Benioff 1-90 system.

Because of the particular slowness of the 1946 event, the computation of  $E^E$  was performed over a time window of variable length,  $t_d$ , generally longer than the 70 s specified by Newman & Okal (1998). Also, following Weinstein & Okal’s (2005) study of the 2001 Peruvian earthquake, we examined the possibility of a late source by delaying the onset  $t_b$  of the time window. As a result, we contour in Fig. 9 the values of  $E^E$  as a function of  $t_b$  and  $t_d$ , the former being referred to the theoretical  $P$  arrival time, 12:36:13 GMT. This diagram suggests an estimated energy  $E^E = 8 \times 10^{21}$  erg, and a minimum duration  $t_d = 160$  s for the contributing wave train after the theoretical arrival time. Note that this inferred duration is in general agreement with the combination of the rise time  $\tau_c = 40$  s derived from the surface wave spectra, of a rupture time  $t_R = \frac{L_R}{V_R} = \frac{120 \text{ km}}{1.12 \text{ km s}^{-1}} = 105$  s

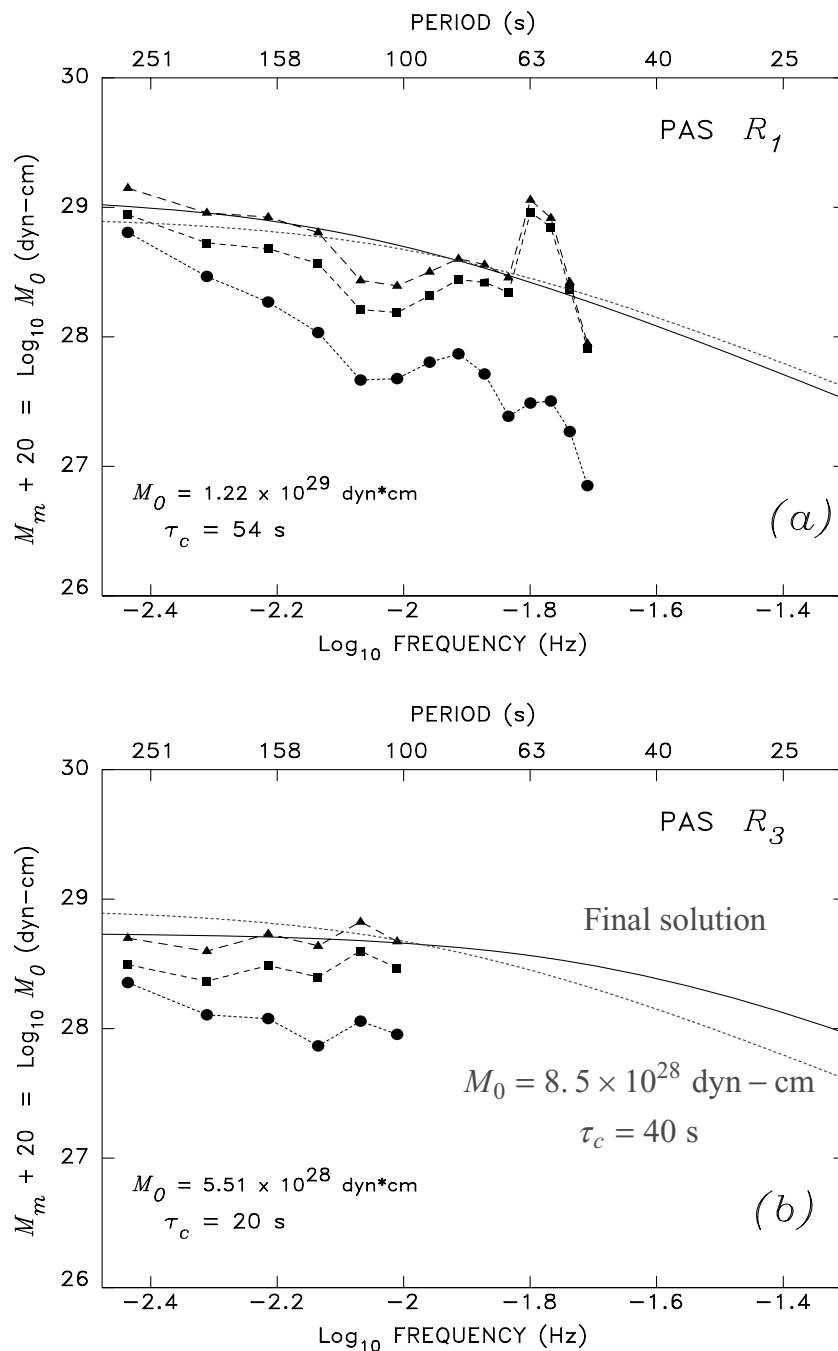


**Figure 6.** (a) Sequence of interpretative corrections to the measurement of  $M_m$  as a function of frequency, in the case of  $R_1$  at Pasadena. The solid dots (and short-dashed line) are computed using the standard correction  $C_S$ , and identical to those values shown in Fig. 5. The squares (with intermediate-length dashes) result from applying the directivity correction (eq. 4). Finally the triangles (joined by the long-dashed line) result from using the exact value of the excitation for a particular focal mechanism and source depth, rather than the average correction  $C_S$ . The solid line is the best fit by an equation of the form (2) (Silver & Jordan 1983) to the set of such corrected values, with  $M_0$  and  $\tau$  listed at lower left. (b) same as above for the phase  $R_3$  at PAS. The dotted red lines are in both cases the final Silver and Jordan source ( $M_0 = 8.5 \times 10^{28}$  dyn-cm;  $\tau_c = 40$  s), best fitted to the full data set of 11 records.

(using the longer arm  $L_2$  of the bilateral rupture and  $V_R$  determined above from the mantle wave spectra), and of a maximum offset of  $\sim 15$  s for the contribution to the generalized  $P$  wave of the phase  $sP$  from the deepest parts of the fault plane. On the other hand, the value of  $E^E$  does not grow substantially if  $t_b$  is increased from  $t_b = 0$ , indicating that the rupture is not delayed as in the case of the 2001 Peruvian earthquake (Weinstein & Okal 2005).

The resulting value of  $\Theta = \log_{10} \frac{E^E}{M_0}$  amounts to  $-7.03$ , the lowest of its kind computed so far for any event (Fig. 10). Thus, the 1946 earthquake is exceptionally slow, significantly more so than tsunami earthquakes such as Nicaragua, 1992 ( $\Theta = -6.30$ ; Newman & Okal 1998), or even the great 2004 Sumatra earthquake [ $\Theta = -5.95$  using the 300 s Harvard moment, and  $-6.35$  if considering the moment derived from normal modes (Weinstein & Okal 2005; Stein & Okal 2005)]. Note that even the use of an extremely conservative value of

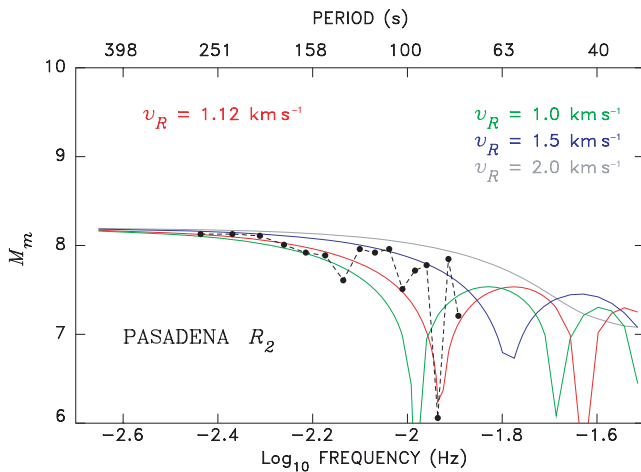


**Figure 7.** Influence of the rupture velocity  $V_R$  on the spectral amplitude of the phase  $R_2$  at Pasadena. Note the pronounced spectral hole at 86.3 s, constraining the velocity  $V_R$  in the geometry  $L_1 = 80$  km,  $L_2 = 120$  km obtained from Fig. 1.

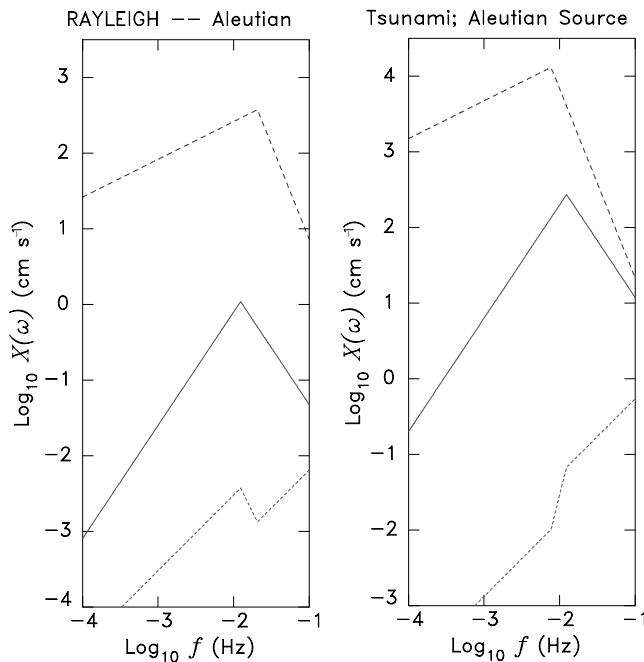


**Figure 8.** Schematic comparison of the excitation of Rayleigh waves (*Left*) and tsunamis in the far field (*Right*) for a seismic dislocation and a landslide. The dashed line represents the excitation predicted for a far field Rayleigh wave in the asymptotic model of Okal (2003) for an earthquake with moment  $8.5 \times 10^{28}$  dyn-cm, and the solid line for the  $200 \text{ km}^3$  landslide used by Okal *et al.* (2003a) to model the near-field tsunami. The dotted line at bottom is the ratio of the two curves. This figure is adapted from Fig. 1 of Okal (2003) by using definitive values for the size of both sources.

only  $10^{28}$  dyn-cm for the 1946 moment would result in  $\Theta = -6.10$ , suggestive of a very slow source.

Finally, we want to emphasize that the low value of  $\Theta$  found here for the 1946 Aleutian event cannot be the result of a systematic bias due to the use of historical records. Indeed, Okal & Kirby (2002) used the same algorithm on a record written by the same instrument (the Benioff 1-90 seismometer at Pasadena) to document a higher than usual  $\Theta = -4.04$  in the case of the 1939 Chile earthquake.

### Recall the absence of $T$ wave

We also recall that the exceptional slowness of the 1946 main shock is confirmed by the absence of a detectable  $T$  wave. We showed in Okal (2004a) that previous identifications of a  $T$  phase on the E–W component of the record of the 1946 Aleutian event written on the Bosch-Omori seismograph at Hawaiian Volcano Observatory (HVO) (Walker & Okubo 1994; Fryer *et al.* 2004) resulted from an erroneous interpretation of time marks on the record, and that the weak  $T$  phase identifiable at HVO was in fact generated by the 12:55 aftershock, rather than the main shock. This observation further stresses the essential difference in rupture properties between main shock and aftershock. Unfortunately, because it takes place in the coda of the main shock, it was impossible to process the main aftershock at 12:55 GMT for  $M_m$  and  $E^E$ , and to further quantify its source properties. Nevertheless, and as documented in detail in Okal *et al.* (2003b) and Okal (2004b), weak or absent  $T$  phases are a trademark of slow events, and in particular of ‘tsunami earthquakes’, as such events are not efficient generators of high-frequency energy. Thus, the absence of  $T$  phase at HVO from the main event, while the 12:55 aftershock generates a detectable one in essentially the same geometry, is comparable to the deficiency in  $T$  phase observed from such slow events as the 1992 Nicaragua and 1996 Chimbote, Peru tsunami earthquakes, when compared to nearby, regular earthquakes (Okal *et al.* 2003b).

### DISCUSSION AND CONCLUSION

The main conclusion of this study is that the seismological data available for the 1946 Aleutian earthquake can be explained by a dislocative source featuring a large, very slow, bilateral rupture. While a landslide may have been triggered by the earthquake, we find nothing in the seismic observables to warrant the suggestion by Fryer *et al.* (2004) that the whole event was a landslide exclusive of a major dislocation, or whose seismic trigger would have been so small as to make it invisible seismically.

The principal properties revealed by our investigations are a static seismic moment  $M_0 = 8.5 \times 10^{28}$  dyn-cm and a fault length of at least 200 km rupturing in a bilateral mode, 80 km towards ENE and 120 km towards WSW, at an average velocity of  $1.12 \text{ km s}^{-1}$ . As illustrated in Fig. 11, this slow bilateral rupture makes the 1946 event the ultimate ‘tsunami earthquake’ in terms of disparity between conventional (or even mantle) magnitudes and potential for tsunami genesis: interference is destructive in all azimuths for all surface waves at typical crustal periods (20 to 50 s) and, even around 120–150 s, Rayleigh waves are strongly affected especially in the well-sampled northeastern azimuths. Only the longest mantle waves ( $\sim 500$  s), which could not be properly recorded by historical instruments, would be immune to the effect of directivity. By contrast, the tsunami directivity pattern features narrow lobes of full positive interference in the azimuths perpendicular to the fault, as the velocity of rupture, although slow by seismic standards, remains hypersonic with respect to the tsunami phase velocity, taken here as  $0.22 \text{ km s}^{-1}$  (Ben-Menahem & Rosenman 1972; Okal & Talandier 1991). The resulting tsunami directivity pattern in the far field is in agreement with the results of Okal *et al.*’s (2002) field surveys.

While the source properties of the 1946 event are unusual, they are not unprecedented. The rupture velocity,  $V_R = 1.12 \text{ km s}^{-1}$  is much slower than that of shear waves in representative crust or upper mantle, but comparable to the values of 1 to  $1.5 \text{ km s}^{-1}$  proposed by Kikuchi & Kanamori (1995) for the 1992 Nicaraguan tsunami earthquake, for which they also advocated a bilateral rupture. Similarly,

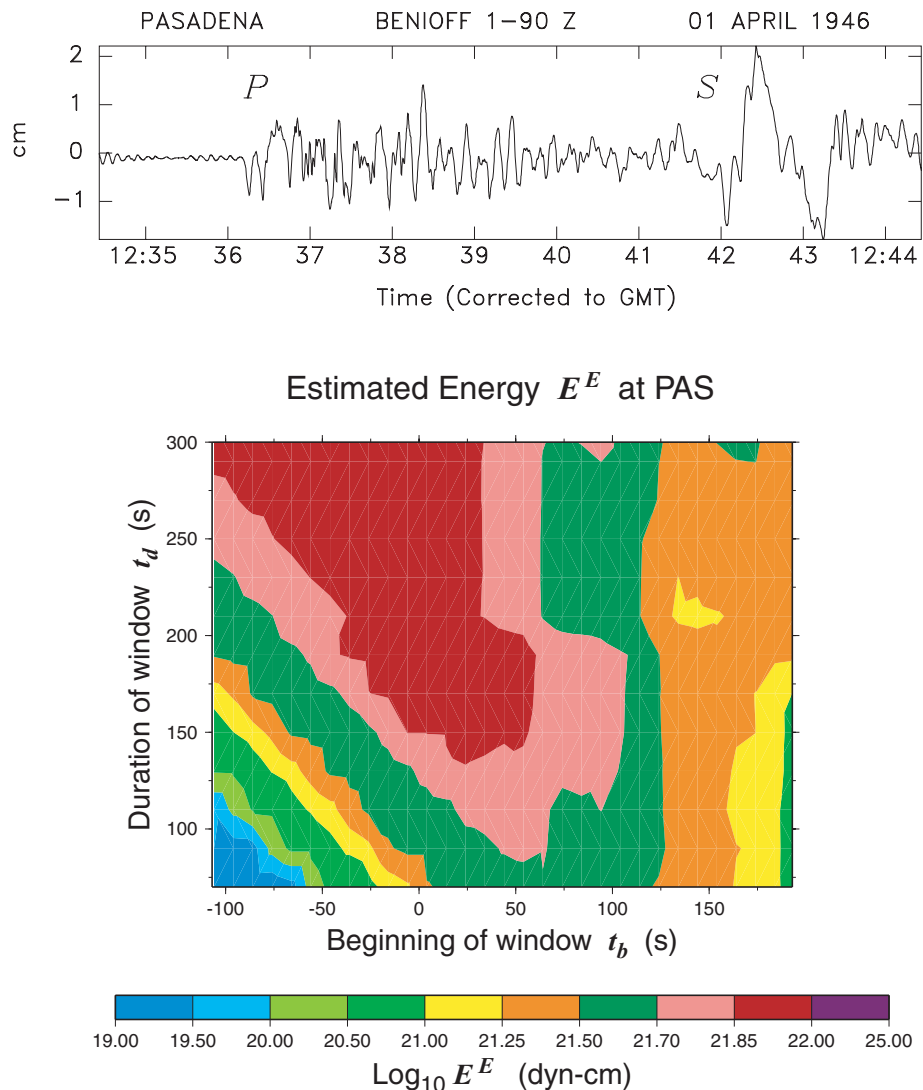


**Figure 9.** Computation of the estimated energy  $E^E$  from the Benihoff 1-90 vertical record at Pasadena. *Top:* Close-up of the waveform, including the  $P$  and  $S$  arrivals. The record extends for 10 min, starting at the original 12:35 min mark (12:34:26 GMT after correction). *Bottom:* Estimated energy  $E^E$  contoured as a function of the beginning of the processing window ( $t_b$ , expressed from the theoretical  $P$ -wave arrival time, 12:36:13 GMT) and of its duration ( $t_d$ ); see text for interpretation.

Velasco *et al.* (1994) obtained low values of  $V_R$  (0.9–2.3 km s<sup>-1</sup>) for the Nicaraguan event, but their model of rupture was essentially unilateral.

In general, low values of rupture velocities ( $V_R \leq 2$  km s<sup>-1</sup>) have been ascribed either to rupture in mechanically deficient media, such as sedimentary wedges in the case of relatively small, aftershock-type, events (Fukao 1979), or sedimentary structures entrained during subduction in the case of the great 1896 Sanriku earthquake (Tanioka & Satake 1996). Alternatively, Tanioka *et al.* (1997) have invoked an erratic, ‘jerky’ progression of the rupture along an irregular, possibly corrugated fault system in sediment-starved environments such as the Nicaraguan trench. It is not clear which of these three models would apply to the Aleutian subduction zone in the vicinity of Unimak, where the oceanic crust is Lower Eocene in age, and thus expected to be much more sedimented than in Nicaragua, but much less so than at the Sanriku Trench.

At  $\Theta = -7.03$ , the energy-to-moment ratio of the 1946 earthquake is the lowest measured to date for any event. Following

Newman & Okal’s (1998) eq. (14), we note that  $E^E/M_0$  is expected to scale like  $(V_R/\beta)^3$ , which, for  $V_R \approx 1$  km s<sup>-1</sup>, correctly predicts a deficiency in  $\Theta$  of 1.5 logarithmic units in the case of the Nicaraguan earthquake (Kikuchi & Kanamori 1995). The additional deficiency in  $\Theta$  observed for the 1946 earthquake could reflect a lower stress drop, which also affects  $E^E/M_0$  through the ratio  $D/W$  of seismic slip to fault width. A reduction of the stress drop to a few bars (from 11 bars as proposed for the Nicaraguan event by Kikuchi & Kanamori 1995) could reconcile the observed value of  $\Theta$ . The combination of a low stress drop and a low  $V_R$  would make the 1946 event the end member, in terms of energy deficiency, of a relatively large population of tsunami earthquakes, whose parameters  $\Theta$  vary essentially continuously from  $-5.8$  to  $-7$  (Fig. 10).

Finally, both the spatial and temporal distribution of the aftershocks of the 1946 earthquake are typical of the patterns observed following a large dislocation: the longitudinal extent of the aftershock zone is essentially doubled from previous studies, leading to a more typical aspect ratio  $W/L$ , approaching 1/2. Most of the

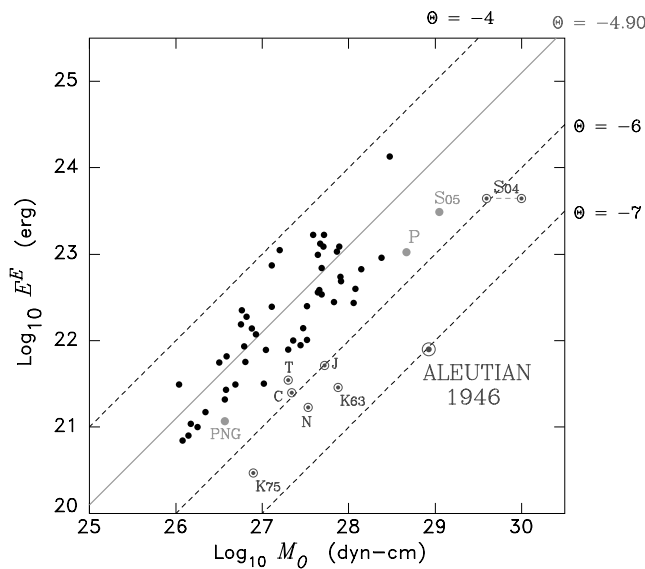


**Figure 10.** Estimated Energy  $E^E$  and parameter  $\Theta$  of the 1946 Aleutian event in relation to the data set of Newman & Okal (1998). This figure is adapted from their Figure 4. The bull's eye symbols show 'tsunami earthquakes', featuring a parameter  $\Theta \leq -5.75$ , identified as 'N' (Nicaragua, 1992), 'J' (Java, 1994), 'C' (Chimbote, Peru, 1996), and 'T' (Tonga, 1982). The data set has been complemented by the 1998 Papua New Guinea earthquake ('PNG'; Synolakis *et al.* 2002), the 2001 Peruvian event ('P'; Weinstein & Okal 2005), and the 2004 ('S04') and 2005 ('S05') Sumatra events. For the 2004 earthquake, the two moments obtained from the CMT solution and from the modelling of the Earth's normal modes (Stein & Okal 2005) are shown and linked by the dashed line. Also shown are the 1975 ('K75') earthquake and 1963 ('K63') aftershock, in the Kuril Islands, processed by Okal *et al.* (2003b) from analogue records. Note the exceptional slowness of the 1946 event, which would qualify as slow even if its moment was grossly underestimated.

transverse dimension of the aftershock zone is located under the large and essentially flat continental shelf, which could not accommodate 'afterslides'. As for the evolution of the aftershocks with time, it follows a traditional modified Omori law with an exponent of 1.12, once again typical of dislocative sources.

Based on the rupture area of 21 000 km<sup>2</sup> inferred from our aftershock relocations, the static moment suggests a slip of 6 m for a mantle rigidity ( $7 \times 10^{11}$  dyn cm<sup>-2</sup>), increasing to 8 m in typical crustal conditions ( $5 \times 10^{11}$  dyn cm<sup>-2</sup>), or even more if the material features a significantly deficient rigidity, as proposed for certain other tsunami earthquakes, such as the 1896 Sanriku and 1975 Kuriles events (Fukao 1979; Tanioka & Satake 1996). These estimates set the stage for hydrodynamic simulations of tsunami run-up amplitudes gathered in the far field by Okal *et al.* (2002). Preliminary computations using a slip of  $\sim 9$  m were able to satisfactorily model run-up in Hilo (Titov *et al.* 2000) and at several sites in the Marquesas Islands (Hébert & Okal 2003; Okal & Hébert 2005).

The final model of the 1946 Aleutian earthquake is thus comprised of a genuine earthquake and a landslide. The earthquake source, documented in the present study as large and slow, can account for the far field tsunami (Okal & Hébert 2005); it reconciles all available seismic observables, in particular the spatial and temporal distribution of aftershocks. The landslide source is necessary to explain the spectacular run-up at Scotch Cap (Okal *et al.* 2003a), but is predicted to contribute insignificantly to both the seismic spectrum and the far-field tsunami (Okal & Hébert 2005).

## ACKNOWLEDGMENTS

This research was supported by the National Science Foundation under Grant Number CMS-03-01054. We are grateful to Ota Kulháněk, Don Helmberger, John Ebel, and Jim Dewey for access to the

## BILATERAL DIRECTIVITY PATTERNS

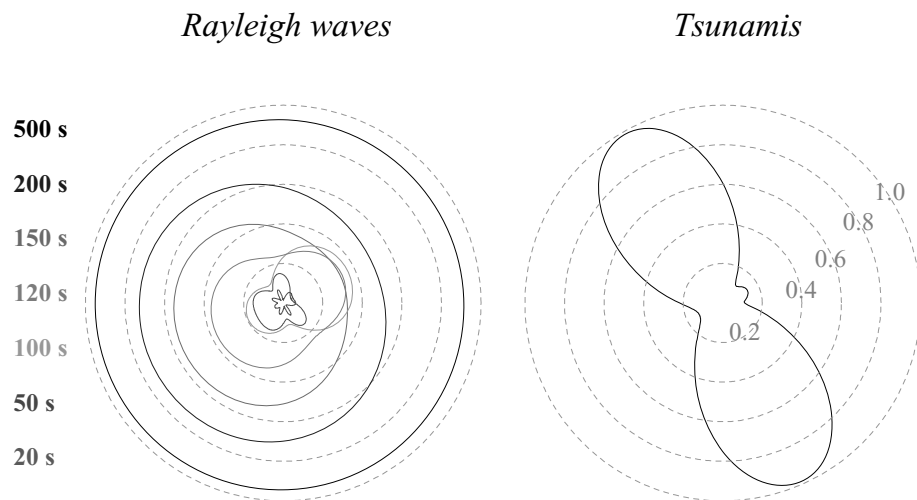


**Figure 11.** Directivity patterns predicted for the bilateral rupture model obtained in this study. On each diagram, the solid lines represent the directivity function  $DIR$  (eq. 3), for  $\phi_R = 63^\circ$ ,  $V_R = 1.12$  km s<sup>-1</sup>,  $L_1 = 80$  km and  $L_2 = 120$  km. In this polar coordinate frame, the outermost dashed line corresponds to  $DIR = 1$ , and the polar angle is the station azimuth  $\phi_s$  with north at top. *Left:* Rayleigh waves at representative periods; *Right:* Tsunamis for  $T = 900$  s.

Uppsala, Pasadena, Weston, and Golden archives, respectively. The paper was improved through the comments of Steve Kirby and another reviewer. Several figures were drafted using the GMT software (Wessel & Smith 1991).

## REFERENCES

- Ben-Menahem, A., 1961. Radiation of seismic waves from finite moving sources, *Bull. seism. Soc. Am.*, **51**, 401–435.
- Ben-Menahem, A. & Rosenman, M., 1972. Amplitude patterns of tsunami waves from submarine earthquakes, *J. geophys. Res.*, **77**, 3097–3128.
- Benioff, H., 1935. A linear strain seismograph, *Bull. Seism. Soc. Am.*, **25**, 283–310.
- Boatwright, J. & Choy, G.L., 1986. Teleseismic estimates of the energy radiated by shallow earthquakes, *J. geophys. Res.*, **91**, 2095–2112.
- Brune, J.N. & Engen, G.R., 1969. Excitation of mantle Love waves and definition of mantle wave magnitude, *Bull. Seism. Soc. Am.*, **59**, 923–933.
- Davies, J., Sykes, L.R., House, L. & Jacob, K., 1981. Shumagin seismic gap, Alaska peninsula: history of great earthquakes, tectonic setting and evidence for high seismic potential, *J. geophys. Res.*, **86**, 3821–3855.
- Fryer, G.J., Watts, P. & Pratson, L.F., 2004. Source of the great tsunami of 1 April 1946: a landslide in the upper Aleutian forearc, *Mar. Geol.*, **203**, 201–218.
- Fukao, Y., 1979. Tsunami earthquakes and subduction processes near deep-sea trenches, *J. geophys. Res.*, **84**, 2303–2314.
- Geller, R.J., 1976. Scaling relations for earthquake source parameters and magnitudes, *Bull. seism. Soc. Am.*, **66**, 1501–1523.
- González, F.I., Mader, C.L., Eble, M.C. & Bernard, E.N., 1991. The 1987–88 Alaskan bight tsunamis: deep ocean data and model comparisons, *Natural Hazards*, **4**, 119–140.
- Gutenberg, B. & Richter, C.F., 1954. *Seismicity of the Earth and associated phenomena*, Princeton Univ. Press, Princeton, New Jersey, 310 pp.
- Hatori, T., 1981. Tsunami magnitude and source area of the Aleutian-Alaska tsunamis, *Bull. Earthq. Res. Inst. Tokyo Univ.*, **56**, 97–110.
- Hébert, H. & Okal, E.A., 2003. Hydrodynamic modeling of the 1946 Aleutian tsunami in the far field using a dislocation source, *Eos, Trans. Am. geophys. Un.*, **84**(46), F810 [abstract].
- Hodgson, J.H. & Milne, W.G., 1951. Direction of faulting in certain earthquakes of the North Pacific, *Bull. seism. Soc. Am.*, **41**, 221–242.
- Jacob, K.H., 1984. Estimates of long-term probabilities for future great earthquakes in the Aleutians, *Geophys. Res. Lett.*, **11**, 295–298, 1984.
- Johnson, J.M. & Satake, K., 1997. Estimation of seismic moment and slip distribution of the April 1, 1946 Aleutian tsunami earthquake, *J. geophys. Res.*, **102**, 11 765–11 774.
- Kajiura, K., 1963. The leading wave of a tsunami, *Bull. Earthq. Res. Inst. Tokyo Univ.*, **41**, 535–571.
- Kanamori, H., 1972. Mechanism of tsunami earthquakes, *Phys. Earth planet. Inter.*, **6**, 346–359.
- Kanamori, H., 1985. Non-double-couple seismic source, *Proc. XXIIIrd Gen. Assemb. Intl. Assoc. Seismol. Phys. Earth Inter.*, p. 425, Tokyo, 1985 [abstract].
- Kikuchi, M. & Kanamori, H., 1995. Source characteristics of the 1992 Nicaragua tsunami earthquake inferred from teleseismic body waves, *Pure appl. Geophys.*, **144**, 441–453.
- Labrousse, Y. & Gilbert, M.J., 1951. Détermination d'un épicerentre à l'aide des couples de stations ayant reçu les ondes *P* à la même heure. Application au tremblement de terre du 1er avril 1946, *Ann. Géophys.*, **7**, 268–271.
- MacDonald, G.A., Shepard, F.P. & Cox, D.C., 1947. The tsunami of April 1, 1946 in the Hawaiian Islands, *Pacif. Sci.*, **1**, 21–37.
- Newman, A.V. & Okal, E.A., 1998. Teleseismic estimates of radiated seismic energy: the  $E/M_0$  discriminant for tsunami earthquakes, *J. geophys. Res.*, **103**, 26 885–26 898.
- Okal, E.A., 1992. Use of the mantle magnitude  $M_m$  for the reassessment of the seismic moment of historical earthquakes. I: shallow events, *Pure appl. Geophys.*, **139**, 17–57.
- Okal, E.A., 2003. Normal modes energetics for far-field tsunamis generated by dislocations and landslides, *Pure appl. Geophys.*, **160**, 2189–2221.
- Okal, E.A., 2004a. Comment on 'Source of the great tsunami of 1 April 1946: a landslide in the upper Aleutian forearc', by G.J. Fryer *et al.*, *Marine Geology*, **209**, 363–369.
- Okal, E.A., 2004b. The generation of *T* waves by earthquakes, *Adv. Geophys.*, in press.
- Okal, E.A. & Talandier, J., 1989.  $M_m$ : a variable period mantle magnitude, *J. geophys. Res.*, **94**, 4169–4193.
- Okal, E.A. & Talandier, J., 1991. Single-station estimates of the seismic moment of the 1960 Chilean and 1964 Alaskan earthquakes, using the mantle magnitude  $M_m$ , *Pure appl. Geophys.*, **136**, 103–126.
- Okal, E.A. & Kirby, S.H., 2002. Energy-to-moment ratios for damaging intraslab earthquakes: preliminary results on a few case studies, *USGS Open File Rept.*, **02-328**, 127–131.
- Okal, E.A. & Hébert, H., 2005. The successful large, slow dislocation and the impossible landslide: modeling the 1946 Aleutian tsunami in the far field, *Proc. Intl. Tsunami Symp., Chania, Greece*, [abstract].
- Okal, E.A. & Synolakis, C.E., 2004. Source discriminants for near-field tsunamis, *Geophys. J. Int.*, **158**, 899–912.
- Okal, E.A., Piatanesi, A. & Heinrich, P., 1999. Tsunami detection by satellite altimetry, *J. geophys. Res.*, **104**, 599–615.
- Okal, E.A. *et al.*, 2002. A field survey of the 1946 Aleutian tsunami in the far field, *Seism. Res. Lett.*, **73**, 490–503.
- Okal, E.A., Plafker, G., Synolakis, C.E. & Borrero, J.C., 2003a. Near-field survey of the 1946 Aleutian tsunami on Unimak and Sanak Islands, *Bull. seism. Soc. Am.*, **93**, 1226–1234.
- Okal, E.A., Alasset, P.-J., Hyvernaud, O. & Schindelé, F., 2003b. The deficient *T* waves of tsunami earthquakes, *Geophys. J. Int.*, **152**, 416–432.
- Pelayo, A.M., 1990. Earthquake source parameter inversion using body and surface waves: applications to tsunami earthquakes and to Scotia Sea seismotectonics, *PhD Dissertation*, Washington University, St. Louis, 254 pp.
- Plafker, G. & Savage, J.C., 1970. Mechanism of the Chilean earthquakes of May 21 and 22, 1960, *Geol. soc. Am. Bull.*, **81**, 1001–1030.
- Polet, Y. & Kanamori, H., 2000. Shallow subduction zone earthquakes and their tsunamigenic potential, *Geophys. J. Int.*, **142**, 684–702.
- Sanford, H.B., 1946. *Log of Coast Guard unit number 368, Scotch Cap DF Station, relating to the Scotch Cap light station tragedy*, 11 pp., US Coast Guard, Washington, DC.
- Scharroo, R., Smith, W.H.F., Titov, V.V. & Arcas, D., 2005. Observing the Indian Ocean tsunami with satellite altimetry, *Geophys. Res. Abstr.*, **7**, 230 [abstract].
- Shepard, F.P., Macdonald, G.A. & Cox, D.C., 1950. The tsunami of April 1, 1946, *Bull. Scripps Inst. Oceanog.*, **5**, 391–528.
- Silver, P.G. & Jordan, T.H., 1983. Total-moment spectra of fourteen large earthquakes, *J. geophys. Res.*, **88**, 3273–3293.
- Stein, S. & Okal, E.A., 2005. Size and speed of the Sumatra earthquake, *Nature*, **434**, 581–582.
- Sykes, L.R., 1971. Aftershock zones of great earthquakes, seismicity gaps, and earthquake prediction for Alaska and the Aleutians, *J. geophys. Res.*, **76**, 8021–8041.
- Synolakis, C.E., Bardet, J.-P., Borrero, J.C., Davies, H.L., Okal, E.A., Silver, E.A., Sweet, S. & Tappin, D.R., 2002. The slump origin of the 1998 Papua New Guinea tsunami, *Proc. Roy. Soc. (London), Ser. A*, **458**, 763–789.
- Tadepalli, S. & Synolakis, C.E., 1994. The runup of *N* waves, *Proc. Roy. Soc. London, Ser. A*, **445**, 99–112.
- Tanioka, Y. & Satake, K., 1996. Fault parameters of the 1896 Sanriku tsunami earthquake estimated from tsunami numerical modeling, *Geophys. Res. Lett.*, **23**, 1549–1552.
- Tanioka, Y., Ruff, L.J. & Satake, K., 1997. What controls the lateral variation of large earthquake occurrence along the Japan Trench?, *Island Arc*, **6**, 261–266.
- Titov, V.V., González, F.I., Mofjeld, H.O. & Newman, J.C., 2000. Short-term tsunami inundation forecasting in Hilo, Hawaii, *Eos, Trans. Am. geophys. Un.*, **81**(48), F757 [abstract].

- Utsu, T., Ogata, Y. & Matsu'ura, R.S., 1995. The centenary of the Omori formula for a decay law of aftershock activity, *J. Phys. Earth*, **43**, 1–33.
- Velasco, A., Ammon, C.J., Lay, T. & Zhang, J., 1994. Imaging a slow bilateral rupture with broadband seismic waves: the September 2, 1992 Nicaraguan tsunami earthquake, *Geophys. Res. Lett.*, **21**, 2629–2632.
- Walker, D.A. & Okubo, P.G., 1994. The *T* phase of the 1 April 1946 Aleutian Islands tsunami earthquake, *Sci. Tsunami Haz.*, **12**, 39–52.
- Weinstein, S.A. & Okal, E.A., 2005. The mantle wave magnitude  $M_m$  and the slowness parameter  $\Theta$ : five years of real-time use in the context of tsunami warning, *Bull. seism. Soc. Am.*, **95**, 779–799.
- Wessel, P. & Smith, W.H.F., 1991. Free software helps map and display data, *EOS, Trans. Am. geophys. Un.*, **72**, 441 and 445–446.
- Wickens, A.J. & Hodgson, J.H., 1967. Computer re-evaluation of earthquake mechanism solutions, *Pub. Dominion Obs. Ottawa*, **33**, 560 pp., Ottawa.
- Wyssession, M.E., Okal, E.A. & Miller, K.L., 1991. Intraplate seismicity of the Pacific Basin, 1913–1988, *Pure appl. Geophys.*, **135**, 261–359.